MECSOL 2022 - Proceedings of the 8th International Symposium on Solid Mechanics
M.L. Bittencourt, J. Labaki, L.C.M. Vieira Jr. and E. Mesquita (Editors), Campinas SP, Brazil, October 17th to 19th, 2022

A Collocation Approach for the Spectral Element Method

N.B.F. Campos [1], J.M.C. Dos Santos [2]

[1] UFABC – Center of Engineering, Modeling and Applied Social Sciences

[2] UNICAMP – College of Mechanical Engineering, Rua Mendeleyev, 200 - Campinas, SP - Brasil

Abstract: The Spectral Element Method (SEM) belongs to a class of Trefftz methods for simulating wave problems in vibroacoustic. The matrices of displacements and forces of this method generally present ill-conditioning, which indeed is common in Trefftz methods. Besides this characteristic, precise results can still be obtained with an advantage over the Finite Element Method due to the reduced dimensions of these matrices. In its original formulation, SEM has no discretization of the boundary. In this work, a collocation approach is used instead. This approach presents results with the same level of accuracy as the original formulation, with the advantage of having faster computational processing. Also, due to the nature of the collocation technique, the boundary conditions are described only at the points chosen, not spamming its restrictions along an infinite line. The formulation implemented is suitable to model rectangular and polygonal Kirchhoff plates, allowing the consideration of several boundary conditions, including mixed ones. Very accurate results were obtained for the cases studied. These results were validated by comparing them with those from FEM models or analytical solutions when available.

Keywords: Spectral Element Method, plates, collocation, high frequency, vibration

INTRODUCTION

The Spectral Element Method (SEM) is a semi-analytic boundary method in whose formulation the exact Fourier series solution for the differential equation in the frequency domain is used as a set of basis functions to describe the field variable. It should not be confused with the Finite Element Method (FEM) formulation that uses high order polynomials and is also referred to in the literature as the Spectral Element Method (Patera, 1984).

The basis functions used in SEM were already introduced by Gorman (1999) to treat the plate bending problem. In his work, he used a combination of several plates, with different boundary conditions, to meet the real boundary conditions of the problem. Kulla (1997) used the same basis functions but adopted a matrix formulation approach to find the coefficients of the homogeneous solution of the plate differential equation. Lee and Lee (1999) used the same approach to model Levy type plates and is the first to denominate this formulation as the Spectral Element Method. Arruda et al. (2004) extended the work of Lee to treat Levy type plates with beam reinforcements in the borders. Campos and Arruda (2008) used the same formulation as Kulla to model beam reinforced plates with arbitrary boundary conditions.

All these studies have in common that the plates modeled needed to be rectangular and the excitations should be applied at the boundary, as prescribed non-homogeneous boundary conditions. The case of domain loads was addressed by modeling the domain with more than one SEM element, making the element interfaces contain the loaded points or lines. By doing so, one of the SEM main characteristics, of being able to model an entire homogenous domain with just one element, could not be used in these cases. Campos and Dos Santos (2015) avoided the need for domain discretization by adding a particular solution to the usual homogenous one used in SEM and then obtaining the general solution of the problem.

Besides being developed for a long time already, the use of SEM to solve practical problems in structural engineering is still very limited, mostly due to the limitations of geometry and loads that can be treated by the SEM formulation in its actual stage of development. This work sets the bases that will allow SEM to be formulated in a more flexible way by using a collocation approach (Huybrechs and Olteanu, 2019) and by adding particular solutions to its traditional formulation to make it possible to apply loads at the plate domain.

Until now, the SEM has been used only to treat problems with rectangular domains. In this work, its formulation is expanded to make it possible to model polygonal plates. This is achieved by discretizing the plate's boundary with arbitrarily collocated points in which the prescribed boundary conditions are enforced.

SEM FORMULATION FOR KIRCHHOFF PLATES

In this section, the SEM formulation for Kirchhoff plates will be derived. First, it will be presented a brief review of the traditional formulation for rectangular domains with loads applied only at the boundary and, in the sequence, a collocation approach is used to solve the problem, which will be extended to cases with domain loads.

Case of rectangular domains

Let us consider a Kirchhoff plate with a rectangular shape with dimension *2a x 2b* and a coordinate system as shown in Fig. 1.

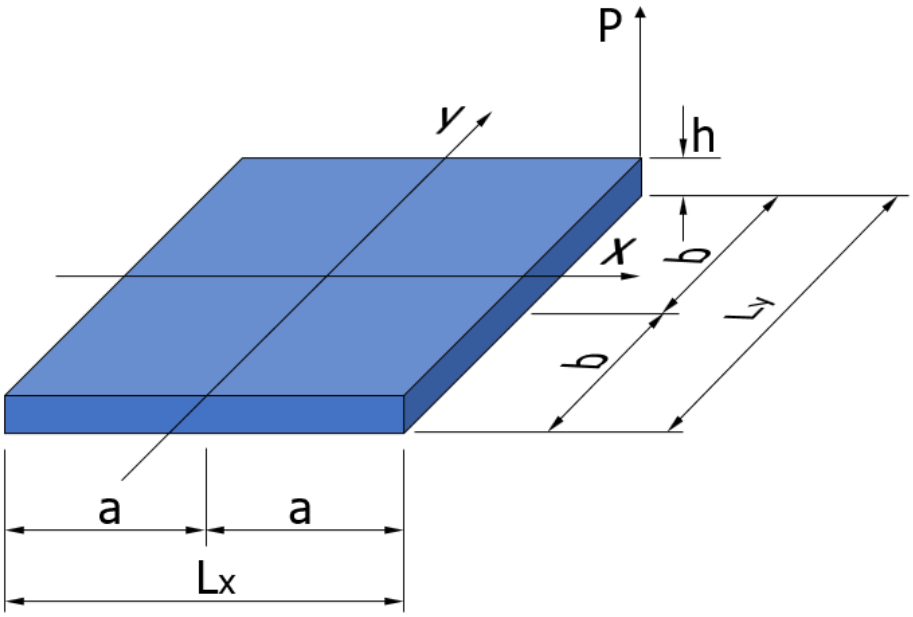

Figure 1: Rectangular Kirchhoff plate

The non-homogeneous differential equation for this plate in the frequency domain has the form:

$$\nabla^4 w - k^4 w = \frac{P(x,y,\omega)}{D} \tag{1}$$

where $D = \frac{E h^3}{12(1-\nu^2)}$ and $k = \sqrt[4]{\frac{\omega^2 \rho h}{D}}$, with h the plate thickness, ρ the material density, υ the Poison's ratio, ω the circular frequency, $P(x, y, \omega)$ a dynamic load, and $w(x, y, \omega)$ the transverse displacement.

The usual formulation of SEM for this problem (Campos and Arruda, 2008) will assume a solution for the homogeneous differential equation in the form $w(x,y;\omega) = C\, e^{px}\, e^{qy}$, with p and q given by:

$$p_{1n} = \pm\sqrt{\left(\frac{n\pi}{b}\right)^2 - k^2} = \pm k_{1xn} \qquad p_{2n} = \pm\sqrt{\left(\frac{n\pi}{b}\right)^2 + k^2} = \pm k_{2xn} \qquad q_n = \pm i\frac{n\pi}{b} \tag{2}$$

$$q_{1m} = \pm\sqrt{\left(\frac{n\pi}{a}\right)^2 - k^2} = \pm k_{1yn} \qquad q_{2m} = \pm\sqrt{\left(\frac{n\pi}{a}\right)^2 + k^2} = \pm k_{2yn} \qquad p_n = \pm i\frac{n\pi}{a} \tag{3}$$

which will produce a set of sixteen basis functions for each value of n. Given **N** terms of the Fourier expansion, the plate transverse displacement will be expressed as

$$
\begin{aligned}
w(x,y;\omega) = \quad & \sum_{n=0}^{N}\left(C_{1n}e^{k_{1yn}y}+C_{2n}e^{-k_{1yn}y}+C_{3n}e^{k_{2yn}y}+C_{4n}e^{k_{2yn}y}\right)\cos\left(\frac{n\pi}{a}x\right)+\ldots \\
& \left(C_{5n}e^{k_{1yn}y}+C_{6n}e^{-k_{1yn}y}+C_{7n}e^{k_{2yn}y}+C_{8n}e^{-k_{2yn}y}\right)\sin\left(\frac{(2n+1)\pi}{2a}x\right)+\ldots \\
& \left(C_{9n}e^{k_{1xm}x}+C_{10n}e^{-k_{1xn}x}+C_{11n}e^{k_{2xn}x}+C_{12n}e^{-k_{2xn}x}\right)\cos\left(\frac{n\pi}{b}y\right)+\ldots \\
& \left(C_{13n}e^{ik_{1xn}x}+C_{14n}e^{-ik_{1xn}x}+C_{15n}e^{k_{2xn}x}+C_{16n}e^{-k_{2xn}x}\right)\sin\left(\frac{(2n+1)\pi}{2b}y\right)
\end{aligned}
\tag{4}
$$

where C_{1n}, ..., $C_{16,n}$ are the unknown coefficients to be determined.

Equation (4), adequately differentiated, can be used to express the boundary conditions in each border of the plate, Eqs. (5)-(10). These bound

$$\phi_x(x,y;\omega) = -\frac{\partial w(x,y;\omega)}{\partial x} \tag{5}$$

$$\phi_y(x,y;\omega) = -\frac{\partial w(x,y;\omega)}{\partial y} \tag{6}$$

$$\mathrm{M}_x(x,y;\omega) = -D\left(\frac{\partial^2 w(x,y;\omega)}{\partial x^2}+\nu\frac{\partial^2 w(x,y;\omega)}{\partial y^2}\right) \tag{7}$$

$$M_y(x,y;\omega) = -D\left(\frac{\partial^2 w(x,y;\omega)}{\partial y^2}+\nu\frac{\partial^2 w(x,y;\omega)}{\partial x^2}\right) \tag{8}$$

$$\mathrm{V}_x(x,y;\omega) = -D\left(\frac{\partial^3 w(x,y;\omega)}{\partial x^3}+(2-\nu)\frac{\partial^3 w(x,y;\omega)}{\partial x\,\partial y^2}\right) \tag{9}$$

$$V_y(x,y;\omega) = -D\left(\frac{\partial^3 w(x,y;\omega)}{\partial y^3}+(2-\nu)\frac{\partial^3 w(x,y;\omega)}{\partial x^2\partial y}\right) \tag{10}$$

In Eqs. (5)-(10), ϕ represents the plate rotations, M the bending moments and V the shear forces.

These equations will then be evaluated at each border and grouped in matrices with dimensions 8xn, containing the force or displacement boundary conditions. The expressions in these matrices are functions of x or y, depending on which edge they are associated with. To remove this dependence, an expansion in the Fourier series is performed at each line, resulting in square matrices containing only Fourier's coefficients.

These matrices can be used to determine the C_n unknown coefficients by solving the linear systems given in Eq. (11)

$$\mathbf{D\,c = d} \qquad \mathbf{F\,c = f} \tag{11}$$

where

$$
\mathbf{D} = \begin{bmatrix}
d_{1,1}^{1} & \cdots & d_{16,1}^{1} & \cdots & d_{1,n}^{1} & \cdots & d_{16,n}^{1} \\
d_{1,1}^{2} & \cdots & d_{16,1}^{2} & \cdots & d_{1,n}^{2} & \cdots & d_{16,n}^{2} \\
\vdots & \vdots & \vdots & \vdots & \vdots & \vdots & \vdots \\
d_{1,1}^{16n} & \cdots & d_{16,1}^{16n} & \cdots & d_{1,n}^{16n} & \cdots & d_{16,n}^{16n}
\end{bmatrix}_{16n\,x\,16n}
\qquad
\mathbf{F} = \begin{bmatrix}
f_{1,1}^{1} & \cdots & f_{16,1}^{1} & \cdots & f_{1,n}^{1} & \cdots & f_{16,n}^{1} \\
f_{1,1}^{2} & \cdots & f_{16,1}^{2} & \cdots & f_{1,n}^{2} & \cdots & f_{16,n}^{2} \\
\vdots & \vdots & \vdots & \vdots & \vdots & \vdots & \vdots \\
f_{1,1}^{16n} & \cdots & f_{16,1}^{16n} & \cdots & f_{1,n}^{16n} & \cdots & f_{16,n}^{16n}
\end{bmatrix}_{16n\,x\,16n}
\tag{12}
$$

$$\mathbf{c} = \begin{Bmatrix} C_{1,1} & \cdots & C_{16,1} & \cdots & C_{1,n} & \cdots & C_{16,n} \end{Bmatrix}^T \tag{13}$$

where $\boldsymbol{D}$ and $\boldsymbol{F}$ are the matrices associated respectively with the displacement and force boundary conditions, $\boldsymbol{c}$ is the vector of unknown coefficients, and $\boldsymbol{d}$ and $\boldsymbol{f}$ the vectors of coefficients obtained by a Fourier expansion of the boundary conditions associated with each plate edge. For mixed boundary conditions, the matrices $\boldsymbol{D}$ and $\boldsymbol{F}$ will also be assembled with mixed terms.

From matrices ***D*** and ***F*,** it is possible to obtain a spectral stiffness dynamic matrix ***S*** by combining Eq. (12) and (13), as shown in Eq. (14)

$$\mathbf{S}\,\mathbf{d} = \mathbf{f} \quad \text{and} \quad \mathbf{S} = \mathbf{F}\mathbf{D}^{-1} \tag{14}$$

Nonetheless, the displacements at any point of the plate can be evaluated by just determining the coefficient's vector ***c*** and introducing it in Eq. (4).

Collocation approach

The main characteristic of the previous formulation is the boundary conditions being defined at infinite lines at each edge of the plate and expressing these boundary conditions by matrices with the Fourier's coefficients used to expand their basis functions. These Fourier's coefficients need to be determined by symbolic computation, resulting in extremely length expressions. A different approach to obtaining matrices ***D*** and ***F*** will be presented here. Instead of defining the boundary conditions at infinite lines, a collocation scheme will be adopted with the boundary conditions being evaluated at discrete points on the plate boundary.

The first step is to define a rectangular region called enclosing box, with dimensions L_x x L_y, that will contain the plate and in which a Fourier expansion will approximate the solution of the plate differential equation. Figure 2 shows three possible valid choices for the enclosing box.

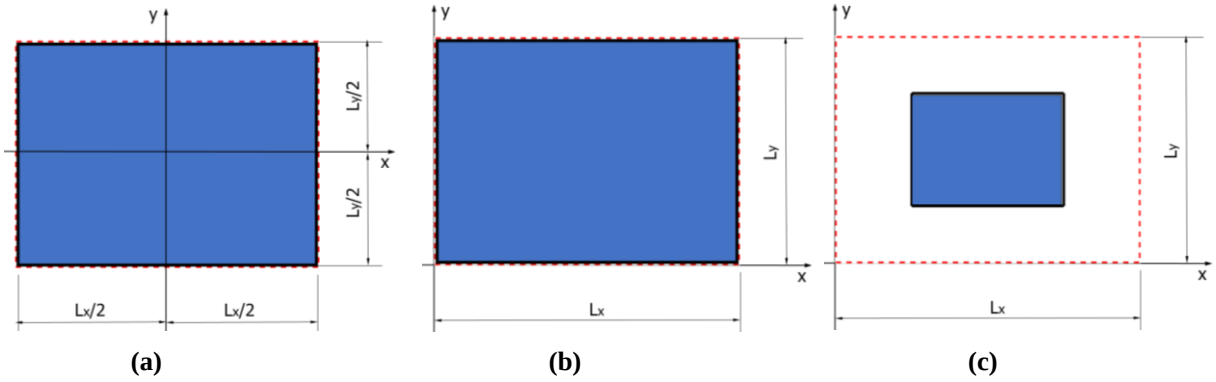

Figure 2: Plate and the associated enclosing boxes

Case (a) corresponds to the enclosing box used in the previous section. For this case, Eq. (4) is still valid and can be used to represent the transverse displacement of the polygonal plate.

In case (b), the plate will be entirely in the first quadrant of the coordinate system and therefore, all plate points will have positive coordinates. This configuration makes it possible to represent the plate transverse displacement by taking just the even components of the Fourier series, with periods $T_x=2L_x$ and $T_y=2L_y$. Equation (4) can then be rewritten accordingly, in a more concise form, and become

$$\begin{aligned} w(x,y;\omega) = \sum_{n=0}^{N}\left(C_{1n}e^{k_{1yn}y} + C_{2n}e^{-k_{1yn}y} + C_{3n}e^{k_{2yn}y} + C_{4n}e^{k_{2yn}y}\right)\cos\left(\frac{n\pi}{Lx}x\right) + \ldots \\ \left(C_{9n}e^{k_{1xm}x} + C_{10n}e^{-k_{1xn}x} + C_{11n}e^{k_{2xn}x} + C_{12n}e^{-k_{2xn}x}\right)\cos\left(\frac{n\pi}{Ly}y\right) \end{aligned} \tag{15}$$

and

$$\begin{aligned} k_{1xn} &= \pm\sqrt{\left(\frac{n\pi}{Ly}\right)^2 - k^2} \qquad k_{2xn} = \pm\sqrt{\left(\frac{n\pi}{Ly}\right)^2 + k^2} \qquad q_n = \pm i\frac{n\pi}{Ly} \\ k_{1yn} &= \pm\sqrt{\left(\frac{n\pi}{Lx}\right)^2 - k^2} \qquad k_{2yn} = \pm\sqrt{\left(\frac{n\pi}{Lx}\right)^2 + k^2} \qquad p_n = \pm i\frac{n\pi}{Lx} \end{aligned} \tag{16}$$

It should be noticed that the left and lower edges of the plate will coincide with the coordinate axis, and for these edges the cosine terms in the expression will have a constant unitary value, and their odd derivatives will be identically null. This can affect the convergence rate of the Fourier series, and more terms will be needed to achieve a solution with good precision.

To avoid this, the enclosing box can be chosen as in case (c), with L_x and L_y having dimensions twice the plate dimensions and with the plate located at its center. By doing so, the basis functions will be richer and the convergence faster. The expression for the transverse displacement of the plate will also be given by Eq. (15), provided that the values of L_x and L_y are chosen accordingly.

It is straightforward to see that this configuration is equivalent to the case (a), with the cosine functions assuming the values of the sine functions of the prior case when $\boldsymbol{n}$ is odd. The only difference with the case (a) is that Eq. (5) will be simpler, since only cosine functions are being used and all the plate points will have positive coordinates. Using only cosine functions does not make obtain the results faster, since it was observed that twice the number of Fourier terms will be needed to achieve the same precision. However, the plate points having only positive coordinates will make the exponential functions with positive exponents assume values that can be excessively high to be represented computationally. This can be avoided with a translation of coordinates for these functions, as it will be explained in the sequence.

Defined the enclosing box and the basis functions associated with it, the next steps are to obtain the expressions for the boundary conditions and to assemble matrices $\boldsymbol{F}$ and $\boldsymbol{D}$. To avoid these matrices depending on x and y, instead of performing a second expansion in Fourier terms, it will be take an evenly spaced arbitrary number of points at the plate boundary, where the expressions of the boundary conditions will be evaluated, Fig. 3. Two points should be considered at the corners or at the interface of different boundary conditions.

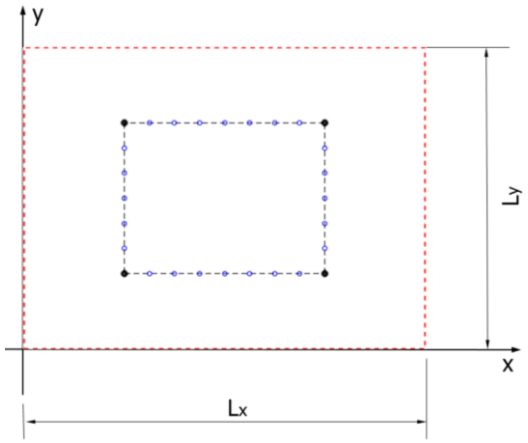

Figure 3: Plate and the associated enclosing boxes

The resulting matrices can be rectangular or square, depending on the number of points taken. The more efficient configuration is to choose enough points to make the matrix square, because in this situation there will be no excess of terms on the basis functions nor in the number of degrees of freedom introduced by the boundary points. In this approach, for polygonal plates, the boundary conditions at the corner points have to be set properly (Paiva, 2018).

The linear system solution

The matrices $\boldsymbol{D}$ and $\boldsymbol{F}$ will usually be ill-conditioned and rank deficient. Even so, high-quality solutions for the linear system can still be achieved. One factor that leads to poor results is that the matrices $\boldsymbol{D}$ and $\boldsymbol{F}$ contain very small and very high values. This problem can be circumvented by scaling the matrices.

The large terms in the matrices come from the exponential functions with positive exponents. Inspection of Eq. (16) shows that the values of the exponents k_{1x}, k_{1y}, k_{2x} e k_{2y} will always have a real part and, if they are positive, large values for the exponentials can arise. This will happen mainly due to these terms depending on the plate dimensions and on the frequency at which it is being excited. Thus, for larger plates and high frequencies, these exponentials will have values excessively high, which can lead to a numeric overflow when trying to solve the problem computationally.

To minimize this problem, the coordinates x and y that appear on these exponentials are translated, as shown in Eq. (17).

$$x' = x - L_x \qquad y' = y - L_y \tag{17}$$

Next, a matrix scaling is performed before solving the corresponding linear system. The common technique of scaling the matrix columns by their norms was not used here to avoid some values becoming too small and then being assumed as being zero by the computational code.

An alternative is to scale the matrix columns by the maximum absolute value present on them. Since the spectral matrix is complex-valuated, this scaling will be done using the maximum real value in each column. Also, the matrix's rows must be scaled, to make all of them have terms of similar magnitude.

Let then $\boldsymbol{M}$ be a complex-valued matrix that can be square or rectangular and $\boldsymbol{S_R}$ and $\boldsymbol{S_C}$ diagonal scaling matrices defined as:

$$\begin{aligned} \mathbf{S_C} &= Diagonal\left(Max\left(Abs\left(Real\left(\mathbf{M}\right)\right)\right)\right) \\ \mathbf{S_R} &= Diagonal\left(Max\left(Abs\left(Real\left(\mathbf{M}\cdot\left(\mathbf{S_C}\right)^{-1}\right)\right)^{T}\right)\right) \end{aligned} \tag{18}$$

and $\boldsymbol{Ms}$ the matrix obtained by scaling $\boldsymbol{M}$

$$\mathbf{M_S} = \left(\mathbf{S_R}\right)^{-1}\cdot\left(\mathbf{M}\cdot\left(\mathbf{S_C}\right)^{-1}\right) \tag{19}$$

Matrices $\boldsymbol{S_R}$ and $\boldsymbol{S_C}$ will scale, respectively, the lines and columns of matrix $\boldsymbol{M}$, making all the terms in matrix $\boldsymbol{M_S}$ have values in the interval [-1,1].

This scaling technique, applied to Eq. (11) gives

$$\mathbf{D_S}\cdot\mathbf{c_S} = \mathbf{d_S} \qquad \mathbf{F_S}\cdot\mathbf{c_S} = \mathbf{f_S} \tag{20}$$

where

$$\mathbf{D_S} = \left(\mathbf{S_R}\right)^{-1}\cdot\mathbf{D}\cdot\left(\mathbf{S_C}\right)^{-1};\quad \mathbf{F_S} = \left(\mathbf{S_R}\right)^{-1}\cdot\mathbf{F}\cdot\left(\mathbf{S_C}\right)^{-1};\quad \mathbf{d_S} = \left(\mathbf{S_R}\right)^{-1}\cdot\mathbf{d}\ ;\ \mathbf{f_S} = \left(\mathbf{S_R}\right)^{-1}\cdot\mathbf{f}\ ;\quad \mathbf{c} = \mathbf{S_C}\cdot\mathbf{c_S} \tag{21}$$

To solve the resulting linear system, the MatLab© software function *lsqminnorm* was used. This function returns a least squares solution for the linear system constrained by the vector of constants determined being the one with the minimum norm. The tolerance used with the function was 1e-8.

The vector $\boldsymbol{c}$ can be determined from the expression of $\boldsymbol{c_S}$ and introduced in Eqs.(5)-(10), (15) to evaluate them at any point of the plate. Residuals calculated for the original linear system are greater than the scaled linear system residuals. This happens because $\boldsymbol{c}$ was obtained from $\boldsymbol{c_S}$ and not directly from solving the original linear system.

Non-homogeneous solution

A general solution $\boldsymbol{w_g}$ for Eq. (1), has the form

$$w_g = w_h + w_p \tag{22}$$

where $\boldsymbol{w_h}$ is the homogeneous solution given by Eq. (4) and $\boldsymbol{w_p}$ is any particular solution.

An effective way to obtain a particular solution for a general loading $\boldsymbol{P(x,y)}$ in the frequency domain, consists of expressing the load in the form of a double sine Fourier series as

$$P(x,y) = \sum_{m=0}^{\infty}\sum_{n=0}^{\infty} B_{mn}\sin\left(m\pi\frac{x}{L_x}\right)\sin\left(n\pi\frac{y}{L_y}\right) \tag{23}$$

with B_{mn} to be determined as usual in Fourier Series expansions.

For the particular case of a point load $\boldsymbol{P(x,y) = P_0\,\delta(x\text{-}x_s)\,\delta(y\text{-}y_s)}$, where P_0 is the magnitude of the load $\boldsymbol{P}$ and $\boldsymbol{\delta(x\text{-}x_s)}$ and $\delta(y\text{-}ys)$ are Dirac's Delta functions, $\boldsymbol{B_{mn}}$ is given by Eq. (24).

$$B_{nm} = \frac{4P_0}{L_xL_y}\sin\left(m\pi\frac{x_s}{L_x}\right)\sin\left(n\pi\frac{y_s}{L_y}\right) \tag{24}$$

where $\boldsymbol{(x_s, y_s)}$ is the point where the load is applied. Accordingly, the transverse displacement $\boldsymbol{w(x_r, y_r)}$ at a point $\boldsymbol{(x_r, y_r)}$ is expressed by

$$w(x_r, y_r) = \sum_{m=1}^{\infty}\sum_{n=1}^{\infty}\frac{4P_0}{L_xL_y}\sin\left(m\pi\frac{x_s}{L_x}\right)\sin\left(n\pi\frac{y_s}{L_y}\right)\sin\left(m\pi\frac{x_r}{L_x}\right)\sin\left(n\pi\frac{y_r}{L_y}\right) \tag{25}$$

Eq. (25) represents a particular solution of the plate and it can be noticed that it is the well-known Fourier Series solution for a point-loaded rectangular simply supported plate with dimensions L_x and L_y, also known as the Navier solution.

Alternatively, a double cosine Fourier series expansion could have been used to find a particular solution as well as mixed cosine and sine functions. Also, any combination of these Fourier series is a particular solution, but it was verified that the results obtained do not improve by combining them, and therefore it is computationally more efficient to use just one of them.

Expressing the plate loading in the form of a Fourier expansion is interesting because this approach can address loads with any shape distribution on the plate domain. However, in the particular case of a point load, it can be found in the literature solutions for thin infinite plates in polar coordinates (Katsikadelis, 2014) (Ianner and Ellermann, 2017) which can be used as particular solutions of the problem, Eq. (26)-(28):

$$w(r) = \frac{P_0}{8\pi D} r^2 \ln r \tag{26}$$

$$w(r) = \frac{iP_0}{8Dk^2}\left(H_0^{(1)}(-rk) + H_0^{(2)}(-irk)\right) \tag{27}$$

$$w(r) = \frac{iP_0}{8Dk^2} \tag{28}$$

where $r = \sqrt{\left(x_s - x_r\right)^2 + \left(y_s - y_r\right)^2}$, and $H_0^{(1)}$, $H_0^{(2)}$ are Hankel functions of the first and second types, respectively.

Equation (26) is the particular solution for the static case, and Eq. (27) and (28) are the particular solutions for the dynamic case with $\boldsymbol{r \neq 0}$ and $\boldsymbol{r = 0}$ respectively. The relations presented in Eq. (5)-(10) and (15) also apply to any particular solution and can be evaluated at all boundary points. These values can be assembled in vectors $\boldsymbol{d_p}$ and $\boldsymbol{f_p}$, in the same order as matrices $\boldsymbol{D}$ and $\boldsymbol{F}$.

$$\mathbf{d_p} = \begin{Bmatrix} \vdots \\ w_{pi} \\ \theta_{pi} \\ w_{p(i+1)} \\ \theta_{p(i+1)} \\ \vdots \end{Bmatrix} \qquad \mathbf{f_p} = \begin{Bmatrix} \vdots \\ V_{pi} \\ M_{pi} \\ V_{p(i+1)} \\ M_{p(i+1)} \\ \vdots \end{Bmatrix} \tag{29}$$

Equation (11) can then be rewritten for the non-homogeneous case as

$$\mathbf{D\,c = d - d_p} \qquad\qquad \mathbf{F\,c = f - f_p} \tag{30}$$

The vector of coefficients $\boldsymbol{c}$ can be found now by solving Eq. (30), after it has been scaled using Eq. (20) and (21), and the solution of the non-homogeneous case is completed.

Numerical results and discussion

To validate the formulation developed in the previous sections, numerical analysis of Kirchoff plates is carried out. Equations (27) and (28) are used as the particular solution and the FRFs are calculated for the same point where the loads are applied. From these FRFs, the MatLab function *pickpoints* will return approximated values for the natural frequencies, which are used in the function *modalfit* to extract the modal parameters and return the natural frequencies in the range where the FRF was calculated. The Operating Deflection Shape (ODS) at these frequencies can then be obtained on points over all the domain and the boundary. Taking the imaginary part of the ODS, normalizing and plotting it will give a result that is very close to the modal shape of the corresponding natural frequency.

For examples 1 and 2 presented in the following, the plate material properties are ρ= 2700 kg/m^3 (density), E=70e9 Pa (Elasticity Modulus), μ=0.3 (Poisson ratio), η=0.1% (damping).

In these two examples, rectangular simply supported plates are evaluated and the results obtained were compared with the Navier solution, Eq. (25), obtained with 100 terms of the expansion. A small and a large plate are modelled to demonstrate that the proposed matrix scaling algorithm is effective in regularizing the matrix and making it possible to have stable results when using SEM independently of the plate's size.

Example 1 – Small Rectangular Simply supported plate

The plate has dimensions L_x = 0.15m, L_y = 0.25m, thickness h=0.001m, and a point load P=1kN applied at point (3a/7, 3b/7). The SEM model has 10 sets of basis functions and 40 boundary points.

Figure 4 shows FRFs obtained using SEM and the Navier solution. They are almost indistinguishable, proving the accuracy of the SEM collocation formulation. Table 1 compares the natural frequencies obtained in the analysis. SEM used a modal extraction technique to identify the natural frequencies from its FRF. From the Navier solution, Eq. (31) was derived and analytically gives all the plate natural frequencies in Hertz. The frequencies obtained using the two methods are almost in perfect agreement.

$$f_{mn} = \frac{\pi}{2}\left(\frac{D}{\rho h}\right)^{1/2}\left(\left(\frac{m}{L_x}\right)^2+\left(\frac{n}{L_y}\right)^2\right),\ m=1,2,3...,\ \ n=1,2,3... \tag{31}$$

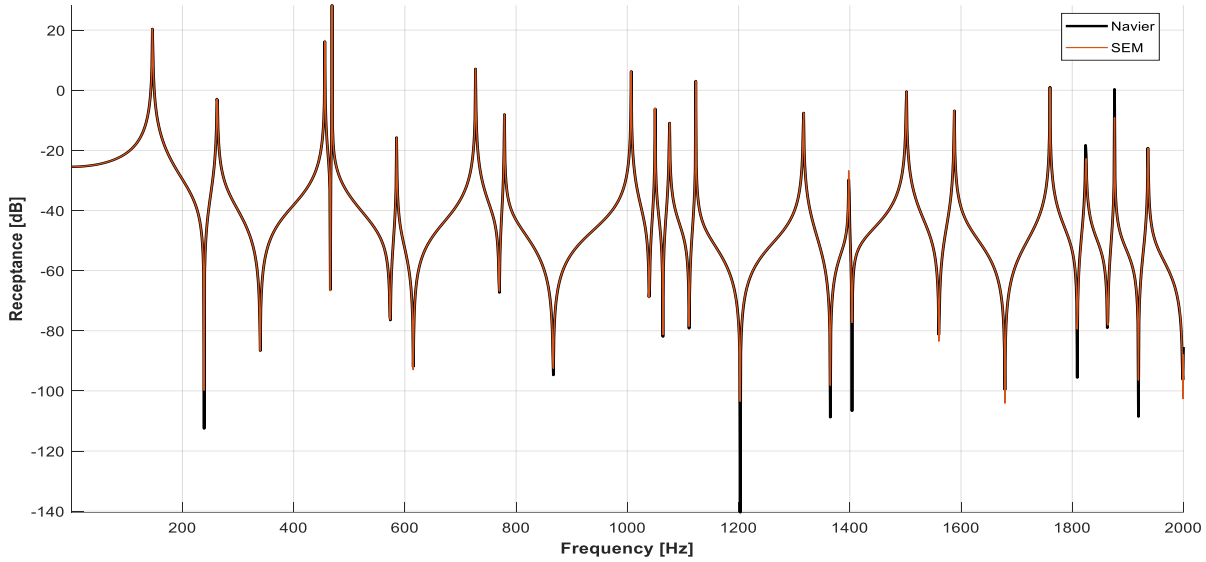

Figure 4: FRFs from SEM and the Navier solution

Table 1: Comparison of natural frequencies from SEM and Navier

Natural Frequencies (Hz)		Error (%)
Navier	SEM	
146.30	146.29	0.004
262.47	262.49	0.007
456.10	456.10	0.000
469.01	469.01	0.001
585.18	585.19	0.001
727.18	727.18	0.000
778.81	778.84	0.004
1006.86	1006.86	0.000
1049.89	1049.90	0.001
1075.71	1075.74	0.003

Natural Frequencies (Hz)		Error (%)
Navier	SEM	
1123.04	1123.04	0.000%
1316.66	1316.66	0.000%
1398.42	1398.17	-0.018%
1501.68	1501.68	0.000%
1587.74	1587.75	0.001%
1759.85	1759.85	0.000%
1824.40	1824.65	0.014%
1876.03	1876.09	0.003%
1936.27	1936.29	0.001%

Figure 5 presents two mode shapes obtained using SEM. It should be noticed that the prescribed boundary conditions are closely met all over the boundary, besides they have been prescribed only at the collocation points.

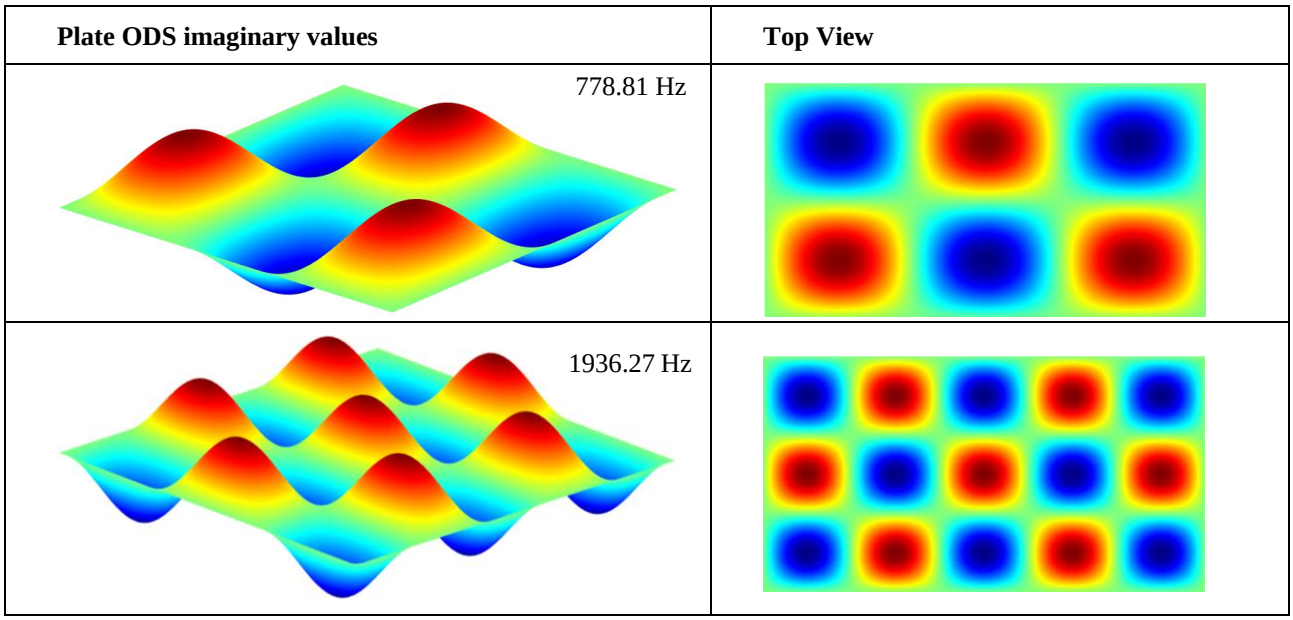

Figure 5: Plate mode shapes from SEM

Example 2 – Large simply supported plate

The plate will have dimensions a=20m, b=30m, thickness h=0.15m, and a point load P=1000 kN applied at point (13a/17, 13b/17). The SEM model has 20 sets of basis functions and 80 boundary points.

Since this plate has a high modal density, the FRF was generated for the frequency range 0 to 50Hz. In Fig. 6 FRFs obtained using SEM and with the Navier solution are shown. They again are in very good agreement, proving that the matrix scaling technique presented in this work makes the SEM formulation robust and stable, being able to be applied to plates with any dimension. without the need for domain discretization.

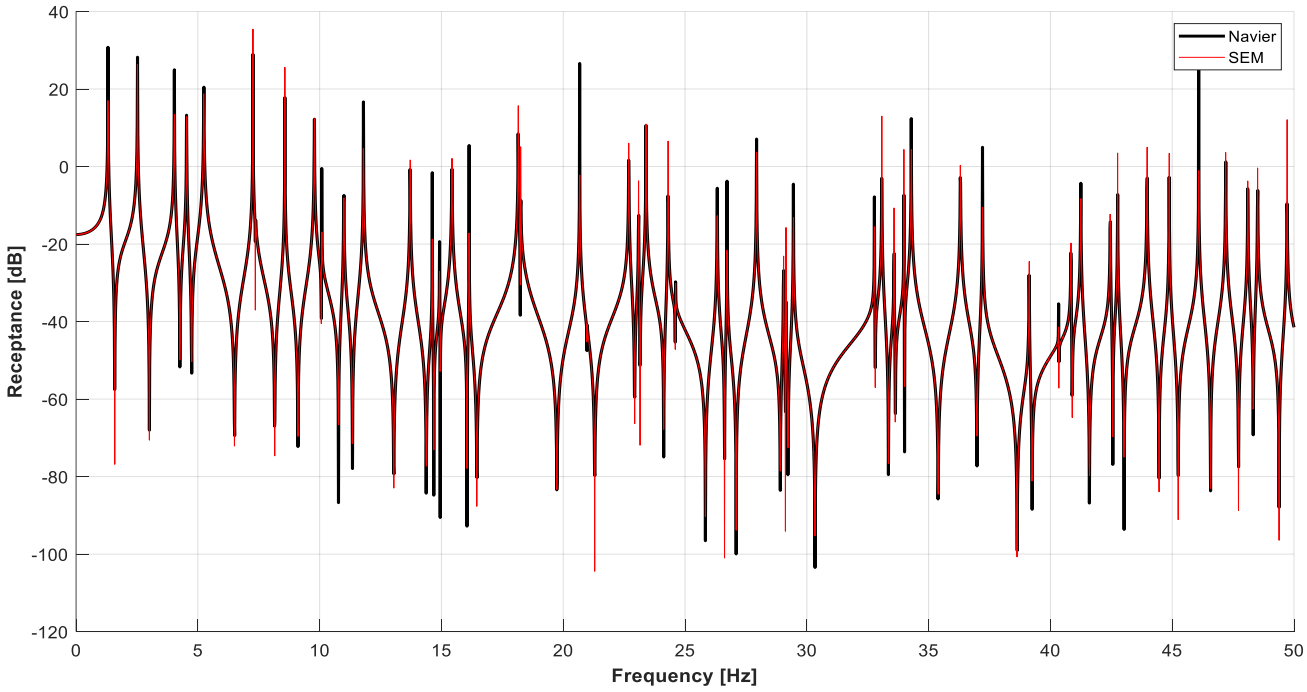

Figure 6: FRFs from SEM and the Navier solution

The natural frequencies obtained are compared in Table 2. Besides the high modal density with 57 corresponding natural frequencies, the agreement between the two methods is still excellent. However, the extraction of modal parameters cannot identify if a natural frequency is associated with two modes of vibration.

able 2: Comparison of natural frequencies from SEM and Navier

Natural Frequencies (Hz)		Error (%)
Navier	**SEM**	
1.31	1.31	0.000
2.52	2.52	0.000
4.03	4.03	0.000
4.54	4.54	0.000
5.24	5.24	0.000
7.26	7.26	0.000
7.36	7.31	-0.679
8.57	8.57	0.000
9.78	9.78	0.000
10.08	10.09	0.099
10.99	10.99	0.000
11.80	11.80	0.000
13.72	13.72	0.000
14.62	14.62	0.000
14.93	14.92	-0.067
15.43	15.43	0.000
16.14	16.14	0.000
18.15	18.15	0.000
18.15	-	-
18.25	18.25	0.000
20.67	20.67	0.000
20.98	20.86	-0.572
22.69	22.69	0.000
23.09	23.09	0.000
23.40	23.40	0.000
24.30	24.30	0.000
24.61	24.62	0.041
26.32	26.32	0.000
26.72	26.73	0.037

Natural Frequencies (Hz)		Error (%)
Navier	**SEM**	
27.93	27.93	0.000
29.04	29.04	0.000
29.14	29.15	0.034
29.45	29.45	0.000
32.78	32.77	-0.031
33.08	33.08	0.000
33.58	33.58	0.000
33.99	33.99	0.000
34.29	34.29	0.000
34.29	-	-
36.31	36.31	0.000
36.31	-	-
37.21	37.21	0.000
39.13	39.13	0.000
40.34	40.31	-0.074
40.84	40.84	0.000
41.25	41.25	0.000
42.46	42.46	0.000
42.76	42.76	0.000
43.97	43.97	0.000
44.88	44.88	0.000
46.09	46.09	0.000
47.20	47.2	0.000
47.20	-	-
48.10	48.1	0.000
48.51	48.51	0.000
48.51	-	-
49.72	49.72	0.000

Two of the mode shapes obtained using SEM are presented in Figure 6. As in the previous example, the prescribed boundary conditions are met very closely all over the boundary.

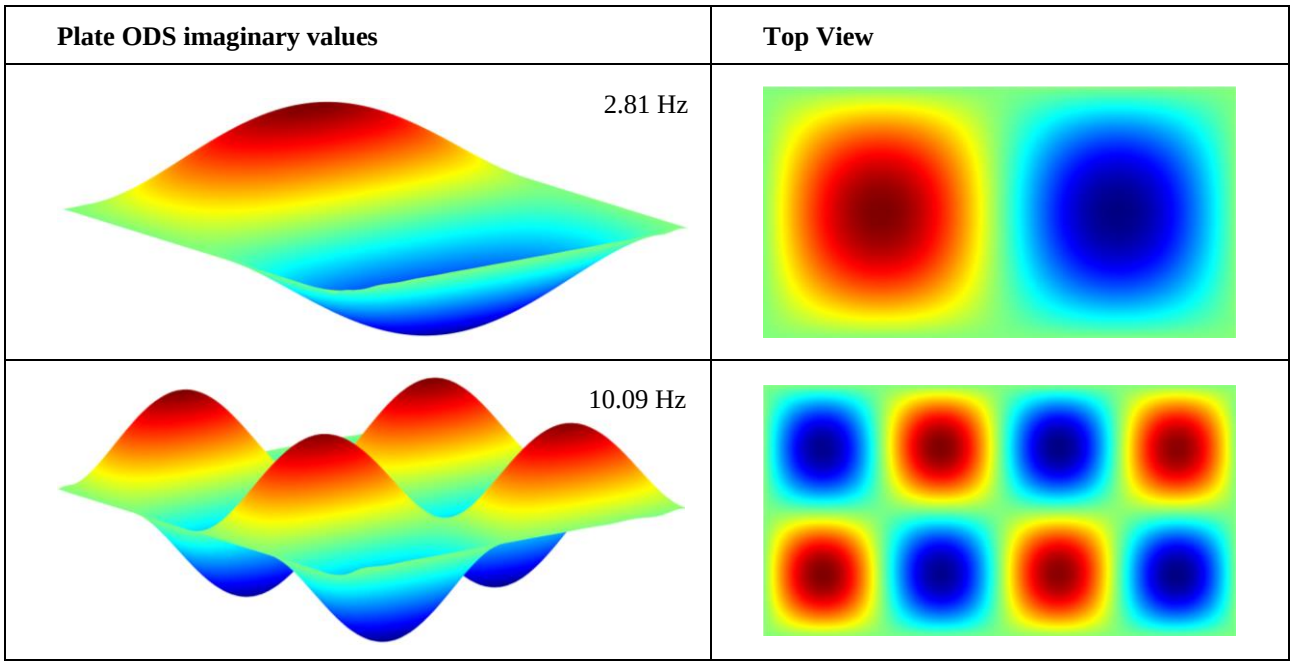

Figure 5: Plate ODS from SEM

Example 3 – Polygonal Simple Supported Plate

The steel plate has an polygonal shape with corners at the points indicated in Fig 7a. and thickness h=0.01m. A point load P=1000 kN is applied at point (x,y)=(1.58, 1.54) m. The plate material properties are ρ= 8750 kg/m^3 (density), E=200e9 Pa (Elasticity Modulus), μ=0.3 (Poisson rate), η=0.1% (damping).

The SEM plate model has 50 sets of basis functions and 200 boundary points, as shown in Fig. 7.

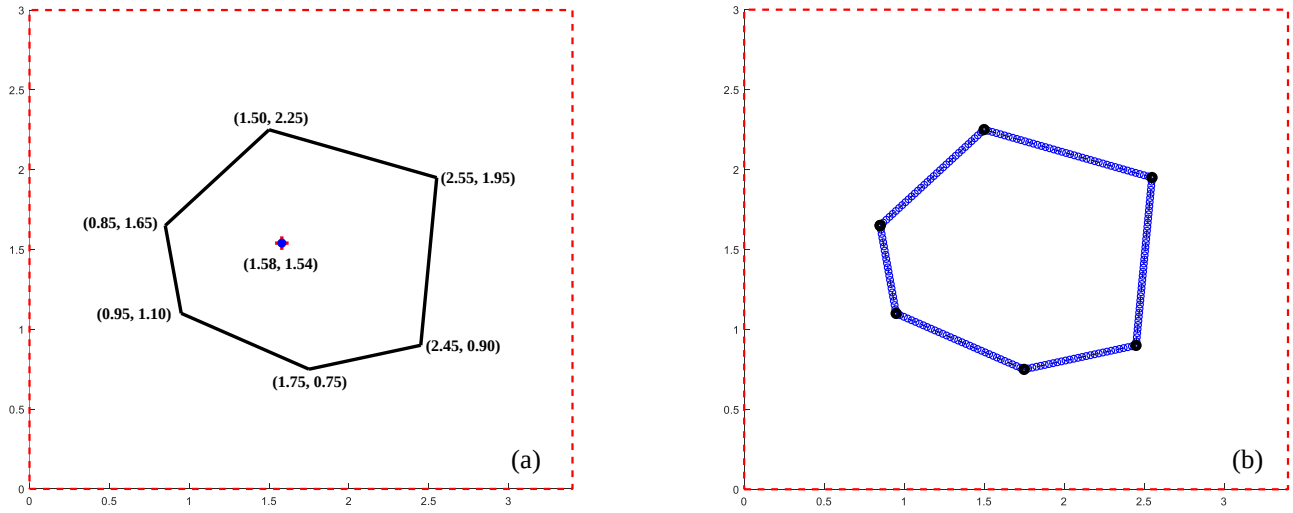

Figure 7: Plate and the enclosing box with (a) point load and (b) boundary points

To access the quality of the results obtained, COMSOL software was used to perform a FEM analysis using a model with triangular elements and 51120 degrees of freedom, as shown in Fig. 8.

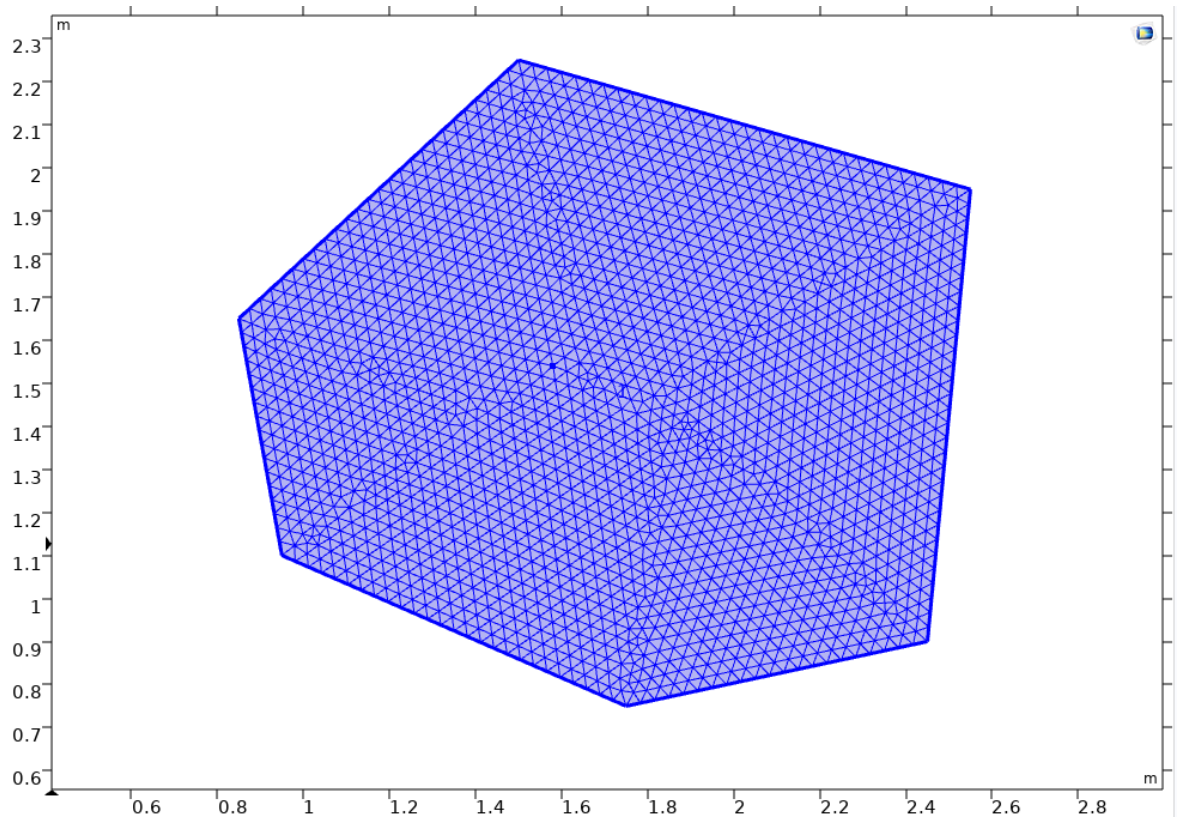

Figure 8: Finite Element Mesh

The natural frequencies below 25 Hz were obtained and compared in Table 3, showing that there is a good agreement between the two methods. In Fig. 9 it is compared two ODSs obtained with the SEM model with the corresponding mode shapes obtained using the FEM model, also showing a good agreement between the two methods.

Table 3: Comparison of natural frequencies from SEM and FEM

Natural Frequencies (Hz)		Difference (%)
SEM	**FEM**	
2,4556	2,5195	-2,538
5,6778	5,7073	-0,517
6,7647	6,8622	-1,421
10,2725	10,3355	-0,609
11,0377	11,0452	-0,068
13,7617	13,8761	-0,824
16,2401	16,2805	-0,248
16,7476	16,8025	-0,326
19,1204	19,1323	-0,062
22,9403	22,9856	-0,197
23,4068	23,5307	-0,527
24,2078	24,2206	-0,053

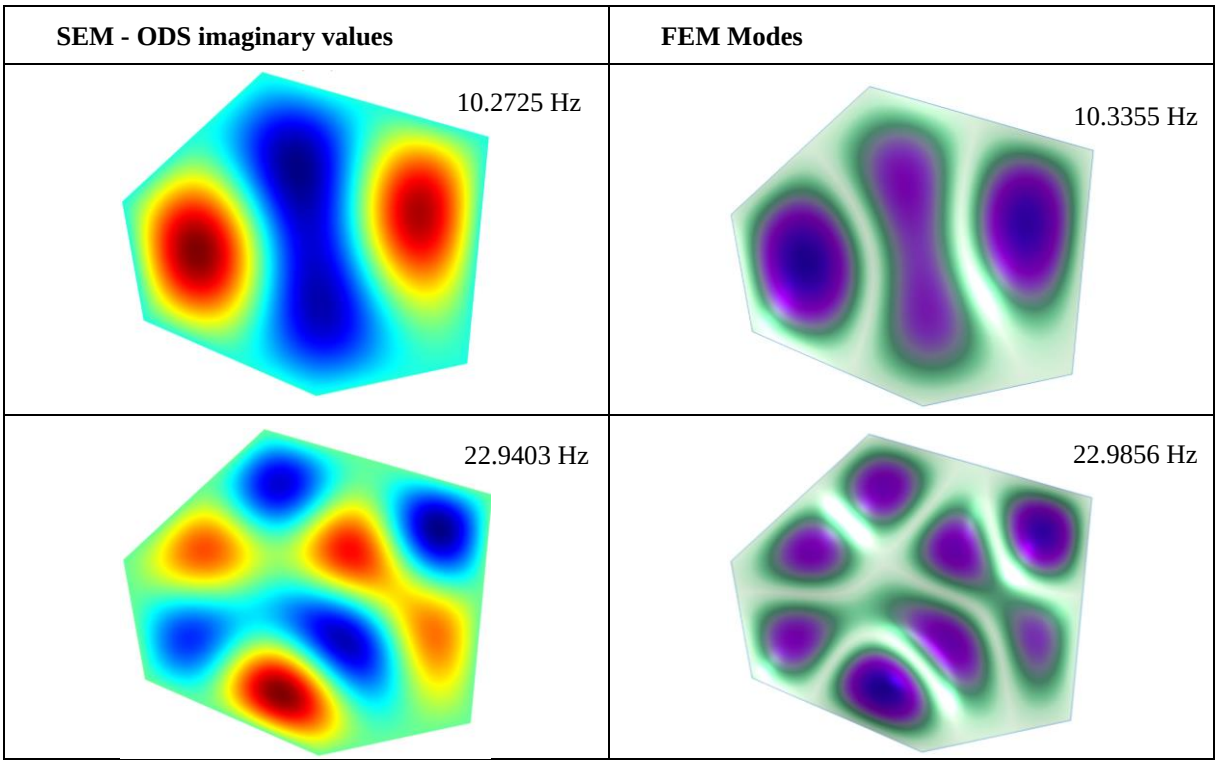

Figure 9: ODS and Modes from SEM and FEM models respectively

CONCLUSIONS AND FUTURE WORK

In this work, it was presented a new formulation of the Spectral Element Method based on a collocation scheme. The numerical examples have proved that this formulation has the same level of accuracy as the traditional SEM formulation, but it is easier to implement and results in faster computational algorithms

These characteristics open a whole new field of research in this subject because makes it possible to use SEM formulation for the modeling of domains with arbitrary polygonal shapes, even no convex ones, making the use of the method much more general. The application of SEM to plates with complex polygonal geometries, including domains with holes and other types of loadings, is being investigated by the authors and very promising results have already been obtained.

These advances in SEM obtained using the collocation approach presented in this work, with the high performance and precision of the method, can make it an excellent alternative in cases where the use of conventional methods is not suitable.

REFERENCES

Arruda, J.R.F., Donadon, L.V., Nunes, R.F. and Albuquerque, E.L., 2004, On the Modelling of Reinforced Plates in the mid-frequency range, INTERNOISE 2004 - The 13th International Congress and Exposition on Noise Control Engineering, Prague, Czech Republic, August 2225.

Campos, N.B.F., ARRUDA, J.R.F., 2008, On the modeling of beam reinforced thin plates using the spectral element method. SHOCK AND VIBRATION, v. 15, p. 425-434. https://doi.org/10.1155/2008/785452

Campos, N.B.F., Dos Santos, J.M.C., 2015, A Spectral Element Method formulation for rectangular thin plates. International Journal of Civil & Environmental Engineering, v. 15, p. 38-44. http://ijens.org/Vol_15_I_02/1511202-4848-IJCEE-IJENS.pdf

Gorman, D. J., 1999, Vibration Analysis of Plates by the Superposition Method (Series on Stability, Vibration and Control of Systems Series a, Volume 3), World Scientific Publishing Company, 270 p.

Huybrechs, D. , Olteanu, A. E. , 2019, An oversampled collocation approach of the Wave Based Method for Helmholtz problems, Wave Motion, Volume 87, April 2019, Pages 92-105. https://doi.org/10.1016/j.wavemoti.2018.06.001

Katsikadelis, J. T., 2014, The Boundary Element Method for Plate Analysis, Elsevier Inc., 1st edition, 2014, pp. 3339.

Kulla, P.H., 1997, “High precision finite elements”, Finite Elements in Analysis and Design 26, pp. 97-114.

Klanner, M., Ellermann, K, 2017, Solutions of Vibration Problems for Thin Infinite Plates Subjected to Harmonic Loads, Journal of Theoretical and Applied Mechanics, 55, 3, pp. 49-961, Warsaw, 2017, https://doi.org/10.15632/jtam-pl.55.3.949

Lee, U., Lee, J., 1999, Spectral-element method of Levy-type plates subjected to dynamic loads, Journal of Engineering Mechanics, February, pp. 243-247.

Patera, A. T., 1984, A spectral element method for fluid dynamics: Laminar flow in a channel expansion. Journal of Computational Physics, Volume 54, Issue 3, June 1984, pp. 468-488. https://doi.org/10.1016/0021-9991(84)90128-1

Paiva, J. B., 2018, Corner restrictions and their application to bending plate analyses by the boundary element method. Engineering Analysis with Boundary Elements, 95, pp. 1-11. https://doi.org/10.1016/j.enganabound.2018.06.012

RESPONSIBILITY NOTICE

The authors are the only parties responsible for the printed material included in this paper.